Cogging-Torque Analysis on Permanent-Magnet Machines by Simulation and Measurement

Christoph Schlensok, Dirk van Riesen, Benedikt Schmülling, Marc Christian Schöning, Kay Hameyer, RWTH Aachen

Manuskripteingang: 03. November 2006; zur Veröffentlichung angenommen: 03. Juni 2007

Cogging torque is an effect to be considered in the design and optimization process of Permanent-Magnet Machines (PMM). Many simulation methods have been proposed. Verification of provided results require measurements of the cogging torque. Measuring it is, though, no easy task. Existing measurement setups often do not decouple the influence of the drive and the measured PMM. Hence, we propose a simple yet accurate test bench design for the measurement of cogging torque. The studied PMM is simulated using the Finite-Element Method (FEM) numerically, and the results are compared.

Keywords: Electrical machines, cogging torque, harmonic analysis, finite-element method

Analyse des Rastmoments von permanentmagneterregten Maschinen mittels Simulation und Messung

Rastmomente müssen bereits im Auslegungsprozess von permanentmagneterregten Maschinen (PMM) berücksichtigt werden. Es gibt eine Vielzahl von Simulationsmethoden. Die Verifizierung von Ergebnissen erfordert eine Messung des Rastmoments. Die Rastmomentmessung ist jedoch keine leichte Aufgabe. Bestehende Messaufbauten entkoppeln meist den Einfluss von Antrieb und PMM nicht hinreichend. Daher wird ein einfacher und genauer Messaufbau zur Messung von Rastmomenten vorgestellt. Eine der untersuchten PMMs wird zudem mittels FEM numerisch simuliert. Die Ergebnisse werden mit denen der Messungen verglichen.

Schlagwörter: Elektrische Maschinen, Rastmoment, harmonische Analyse, Finite-Elemente Methode

1 Introduction

Many studies have been presented concerning the minimization of cogging torque in Permanent-Magnet Machines (PMM) [1–4]. This states the high relevance of the cogging problematic in top-quality PM-servo drives with high-precision positioning ability and for standard mass-produced PMMs as well. Therefore, the determination and estimation of the peak-to-peak cogging torque and the cogging harmonics are of high

interest. Both, simulation and measurement allow for the analysis of the cogging torque. Simulation methods, i. e. the Finite-Element Method (FEM), are well known and easy to apply [5; 6]. Hence, the focus lies on the development of a precise but simple measurement setup allowing for accurate cogging-torque analysis.

Various test-bench setups have been presented or are sold commercially. Nevertheless, there is at least one disadvantage to these. The setup presented in [8] consists of the PMM, a torque transducer and a hydraulic motor as drive. This configuration promises a very high accuracy of the rotor movement. There is no cogging or torque ripple in the hydraulic drive. Nevertheless, the setup works without any offset, so that the measurement is performed in a close range around the zero point. Next to this small disadvantage there is the cost aspect. Hydraulic drives are rather expensive and not easy to handle. Another setup, similar to the one presented in this paper, shows accurate performance but also includes the problem of measuring around "0" [9]. A third alignment is very simple and rather inaccurate. The cogging is measured by weights adjusted for each of the cogging positions [10]. There are a lot of unknown errors in this measurement setup.

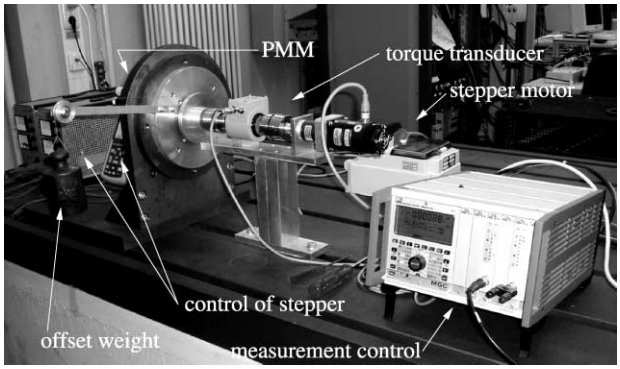

Figure 1: Picture of the measurement setup in the lab.
Bild 1: Foto des Prüfstandes im Versuchslabor.

2 Measurement Setup

The measurement setup is shown in Fig. 1. The PMM is mounted onto a flange and is connected with two flexible couplings to the torque transducer, a gear, and a stepper motor. Between the first coupling and the PMM there is a disc which holds a spindle with a weight. The weight is used as offset torque. This way the measurement is performed in the range of about 1 Nm. The weight's mass is 2 kg and the disc has a radius of 5 cm. The offset allows the torque transducer to measure in its optimum scale range. The transducer's maximum torque is 2 Nm. The signal from the trans-

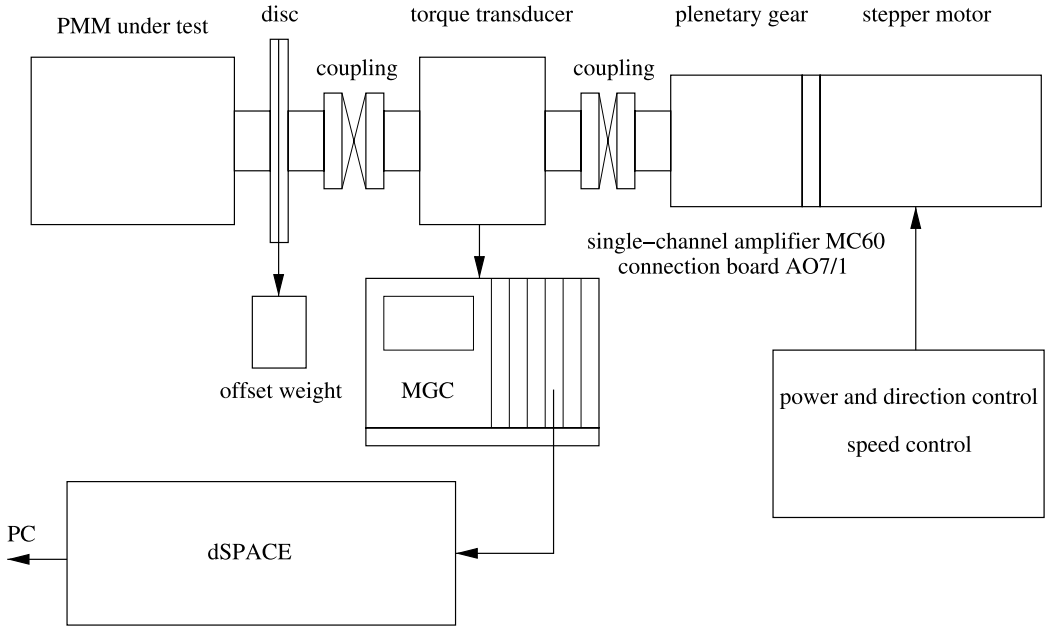

Figure 2: Scheme of the measurement setup.
Bild 2: Schema des Messaufbaus.

ducer is fed into a measurement control unit (MGC) for digital signal processing, e. g. dSPACE [11].

The stepper motor driving the whole setup is controlled by two voltage sources. The resolution of the stepper motor can be switched from $^1/_1$, $^1/_2$, $^1/_4$ to $^1/_8$. By additionally varying the voltage from 0 to 8 V the speed can be adjusted from 0 to 64 rpm with a transmission ratio of the gear of $^1/_{400}$. This high ratio avoids a measurable impact of the stepper motor's torque ripple to the cogging torque of the PMM. The harmonics of the stepper motor are at very high ranges and are filtered from the signal digitally by the software. Figure 2 summarizes the setup schematically.

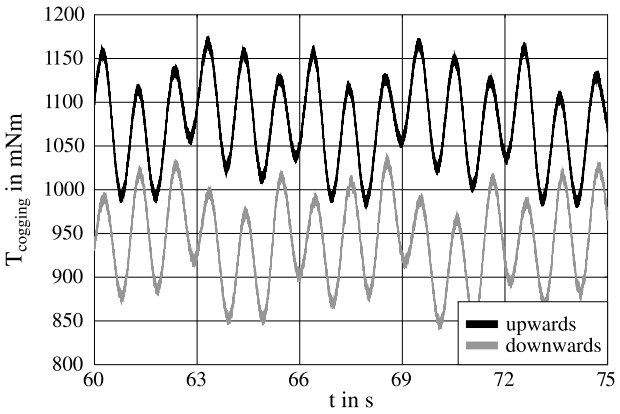

Figure 3: Measured cogging torque for both directions of stepper motor.
Bild 3: Gemessener Rastmomentverlauf für beide Drehrichtungen des Schrittmotors.

Due to the offset weight the average values of the measurements differ with the direction of rotation. Figure 3 shows exemplarily the results for one PMM. It can be stated, that the friction is measured as well. The deviation of the average values of both measurements equals twice the friction of the entire setup. Since the friction acts in the same direction in both cases upwards and downwards, respectively. While the weight is spun upwards the friction works against the torque of the stepper motor. When the weight is moving downwards the friction works in the same direction.

Figure 4 shows the corrected cogging-torque signal without friction and offset. The difference of the resulting time-dependent cogging-torque stems from the rotational direction of the stepper motor. Hence, both measurements are in very good agreement.

3 Measurement Results

The measurement setup is tested with two different servo drives. Both are permanent-magnets synchronous machines. The setup allows three complete rotor revolutions. This depends on the height of the test bench, since the weight is lowered until it touches the floor. For both PMMs the cogging torque is measured at $n = 1$ rpm in both directions of weight movement. As studies have shown the selected speed of the stepper motor leads to accurate results, and an acceptable duration of $T = 3$ min of each of the measurements with an easy handling. Therefore, four different measurements

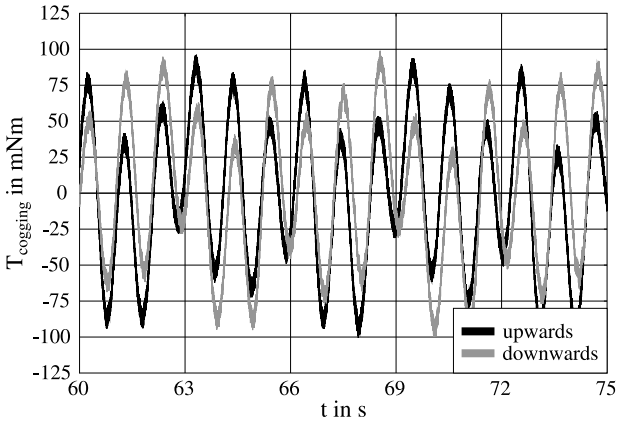

Figure 4: Measured cogging torque without offset and setup friction.
Bild 4: Gemessener Rastmomentverlauf ohne Offset und Reibung.

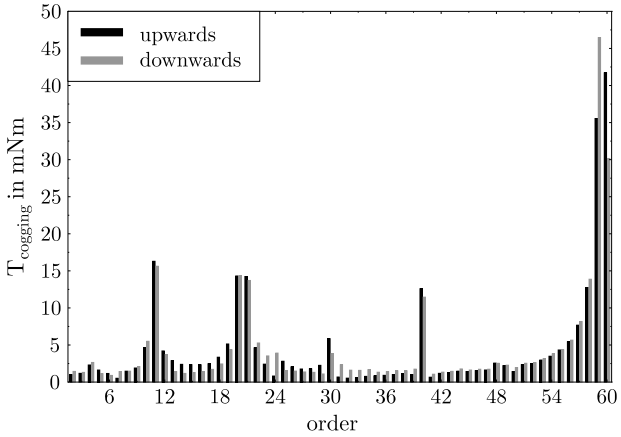

Figure 5: Spectrum of the measured cogging torque for studied PMM A.
Bild 5: Spektrum des gemessenen Rastmomentverlaufs der Maschine PMM A.

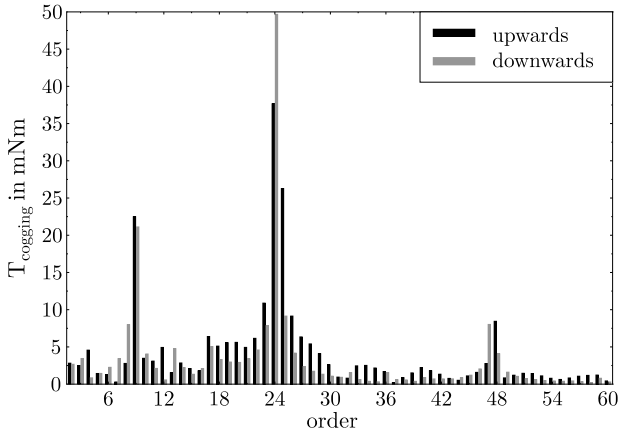

Figure 6: Spectrum of the measured cogging torque for studied PMM B.
Bild 6: Spektrum des gemessenen Rastmomentverlaufs der Maschine PMM B.

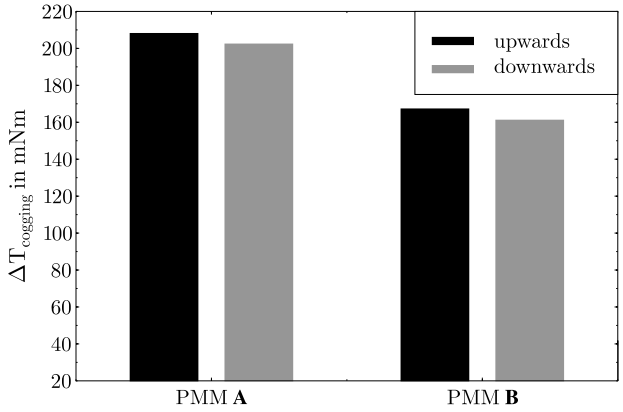

Figure 7: Measured peak-to-peak cogging-torque values.
Bild 7: Spitze-Spitze-Werte der gemessenen Rastmomentverläufe.

need to be performed (upwards and downwards for both PMMs).

Two different cogging-torque analysis criteria are usually applied:

1. The harmonic analysis of the cogging torque, and
2. The peak-to-peak value of the cogging torque.

Both analysis criteria require one complete rotor revolution.

At first the spectra of the four cogging-torque behaviours are analysed. They are depicted in Figs. 5 and 6. For both machines the harmonics are nearly independent of the rotational direction of the stepper motor and match very well. Due to the different designs of both PMMs the harmonics occurring differ. For PMM A the dominant harmonic is order number $O = 60$. PMM B shows major mode number $O = 24$.

The peak-to-peak values of the cogging torque are shown in Fig. 7. It can be stated, that for each of the PMMs the results are allmost independent of the rotational direction. PMM B has a lower cogging torque ($\Delta t = -19.95\%$).

The measurement setup has been used to compare the cogging-torque behaviour of the two PMMs, regarding them as "black boxes", since no construction data was available. Hence, no numerical simulation could be performed, since the stator lamination design is unknown, as are the rotor lamination and size and placement of the permanent magnets. Nevertheless, the measurement states differences between both machines, which could be used as a benchmark for applications where low cogging torque is a requirement.

Next, a different PMM (PMM C) is measured. For this machine, detailed drawings are available. Therefore, the measurements are compared to numerical simulation results, applying the Finite-Element Method (FEM). The machine is measured with the same measurement setup.

Again, a speed of $n = 1$ rpm is chosen, and the upward and downward movement of the counterweight is measured (resulting in clockwise and counter-clockwise rotation of the machine). Figure 8 shows the measured torque values. It must be noted, that the curves are phase-shifted against each other, since the exact starting angle of the machine is not recorded and varies between measurements. But this has no effect on the determination of the peak-to-peak value or the spectrum analysis of the cogging torque.

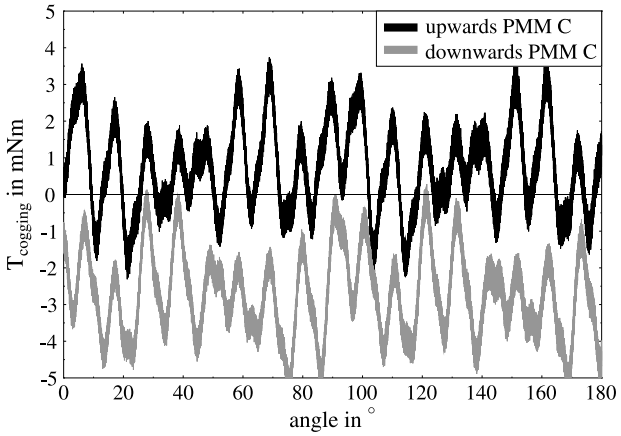

Figure 8: Cogging torque measured in both directions for the PMM C.
Bild 8: Gemessener Rastmomentverlauf der Maschine PMM C.

The friction is eliminated from the measured cogging torque. The resulting time-dependent cogging torque is shown in Fig. 9, which will serve as the starting point for the FFT analysis.

The FFT is performed, resulting in the spectrum depicted in Fig. 10. The most relevant order appearing in the spectrum is $O_{fundamental} = 18$, which is in good agreement with the results expected from the analytical analysis by

$$O_{fundamental} = \mathrm{LCM}(N_S, 2p) = \mathrm{LCM}(18, 6) = 18\,. \qquad (1)$$

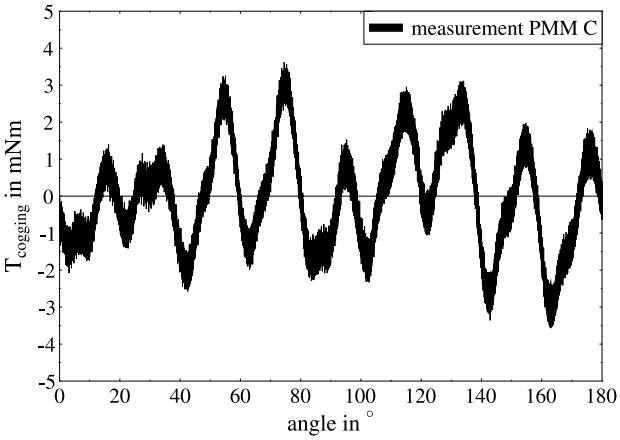

Figure 9: Measured cogging torque for PMM C with friction eliminated.
Bild 9: Gemessener Rastmomentverlauf ohne Offset und Reibung der Maschine PMM C.

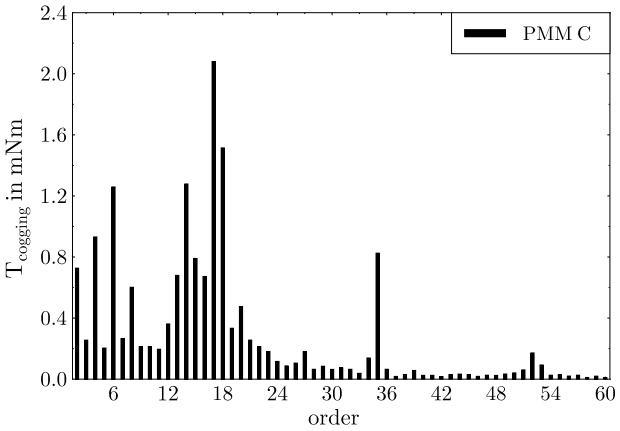

Figure 10: Spectrum of the measured cogging torque for PMM C.
Bild 10: Spektrum des gemessenen Rastmomentverlaufs der Maschine PMM C.

18 is the least common multiple LCM of the number of slots $N_S = 18$ and the number of rotor poles $2p = 6$ (see next section). The 36th order is also clearly visible. Lower orders appear as well, due to asymmetries in the construction.

4 Simulation Results

The numerical electromagnetic simulation is applied to verify both the measurement setup and the FE-model. The solver tool used is iMOOSE [7] which has been developed at the Institute of Electrical Machines at RWTH Aachen University in the past few years. The PMM C is used for the simulation. It consists of $N_S = 18$ stator teeth and $2p = 6$ rotor poles. The lamination is shown in Fig. 11. The permanent magnets are surface-mounted, positioned asymmetrically, and shaped. The 2-dimensional FE model is generated using ANSYS [12]. It consists of about $E = 40\,000$ triangular elements and $N = 20\,000$ nodes. As studies have shown, this mesh density suites the task of calculating such small values of cogging torque. For the simulation a static solver is applied taking rotational movement of the rotor into consideration [7]. The stepping angle between two simulation time steps is $\alpha = 1°$. For each of the $N = 360$ simulation time steps the flux density distribution is provided (Fig. 12).

Due to the high magnetization of the magnets (remanence $B_R = 1.23\,\mathrm{T}$) the flux density reaches significant saturation values in six of the stator teeth for the depicted rotor position. The mounting kerfs on the outer circumference of the stator are distributed asymmetrically. This results in a slightly asymmetric flux

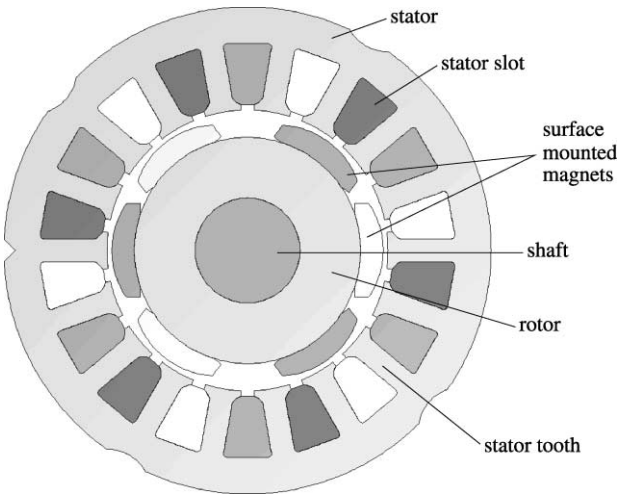

Figure 11: Lamination of the studied PMM C.
Bild 11: Blechschnitt der Maschine PMM C.

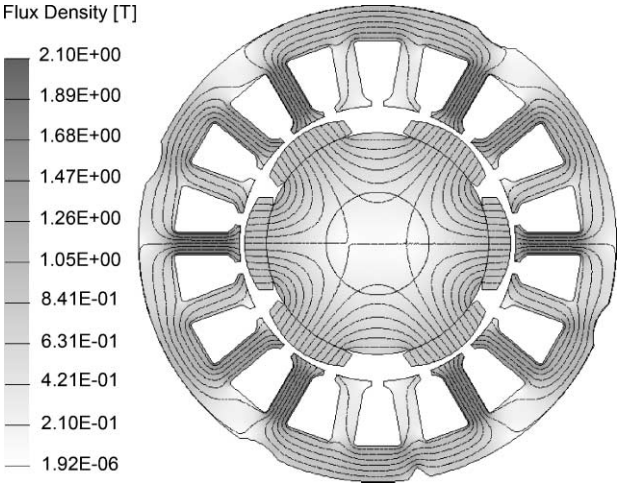

Figure 12: Flux density distribution for a single simulation time step of the FE model.
Bild 12: Induktionsverteilung für einen Simulationszeitschritt des FE-Modells.

distribution in rotor and stator. Due to this asymmetry cogging torque will appear. Depending on the position of the rotor this cogging torque increases significantly.

From the flux-density distribution of each simulation time step the cogging torque is calculated. Figure 13 shows the resulting time depending cogging-torque behaviour. The peak-to-peak value of the cogging torque is $\Delta T = 9.3\,\mathrm{mNm}$. This states that the studied PMM has been designed very accurately.

When simulating the cogging torque, some considerations have to be taken into account. The torque in the simulation is calculated using Maxwell's stress tensor:

$$T = \frac{l_m}{\mu_0} \int_{\Gamma} r \cdot B_r \cdot B_t \cdot \mathrm{d}\Gamma\,, \tag{2}$$

where B_r and B_t are the radial and tangential component of the flux density, Γ a closed surface around the rotor and l_m the length of the machine.

According to [13], the accuracy of torque calculations with Maxwell's stress tensor depends basically on two factors. First, the discretization density must be sufficiently small to be able to resolve the spectrum accurately, and yield an accurate solution with a small error. Secondly, the integration contour position has to be chosen carefully. The air-gap is divided into three layers, which correspond to the stator air-gap, the rotor air-gap and the central air-gap. It is known that the proximity of the integration contour to the steel can lead to significant errors in the torque calculation. Thus, the central air-gap is chosen to include the integration contour. Nevertheless, significant differences in the torque computation occur if the contour is located close to the border of the air-gap layer. Figure 14 shows the torque evaluation in different positions in the air-gap. The curve in the center of the results is also the one in the center position in the air-gap. The two positions which are closer to the stator lamination (higher values of r) show a very large content of higher harmonics. Nevertheless, this is not covered by the theory. Thus, the level of confidence of these results is low. Even comparing the measurement and the simulation for the position in the center of the air-gap, the content of higher orders

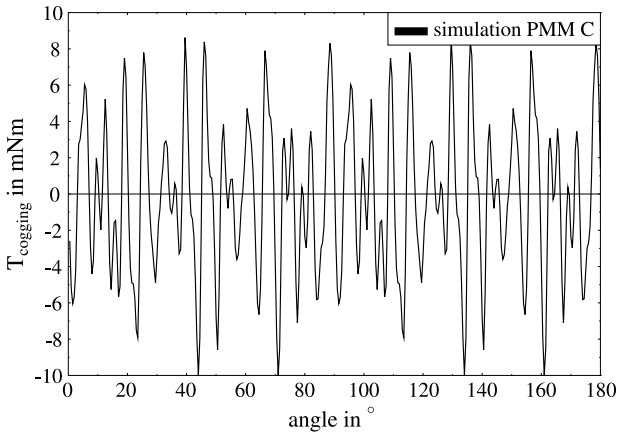

Figure 13: Time-dependent cogging-torque behaviour of the FE model.
Bild 13: Zeitabhängiger Rastmomentverlauf des FE-Modells.

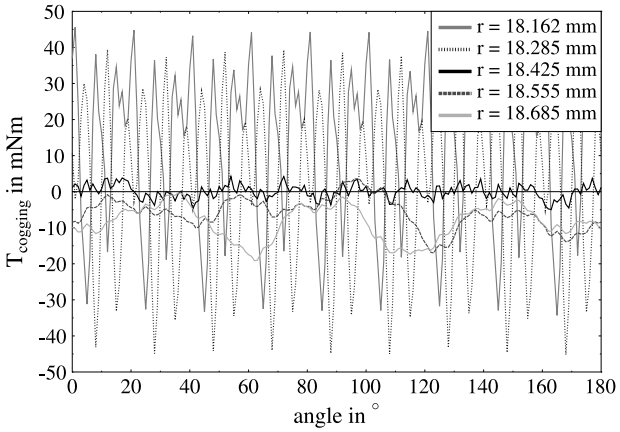

Figure 14: Time-dependent cogging-torque behaviour of the FE model depending on the calculation radius r.
Bild 14: Zeitabhängiger Rastmomentverlauf des FE-Modells in Abhängigkeit vom Berechnungsradius.

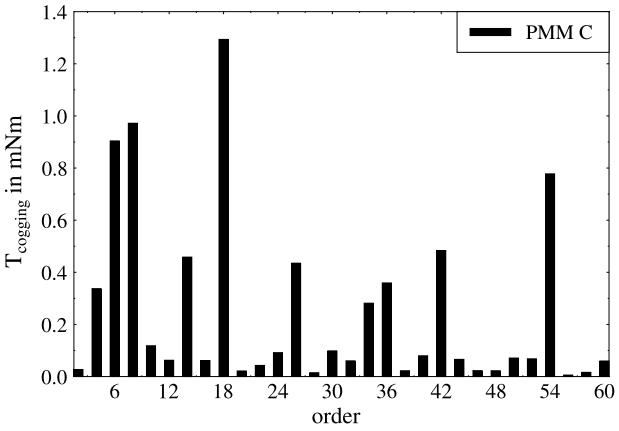

Figure 15: Spectrum of the cogging-torque harmonics of the FE model.
Bild 15: Spektrum der Rastmomentharmonischen beim FE-Modell.

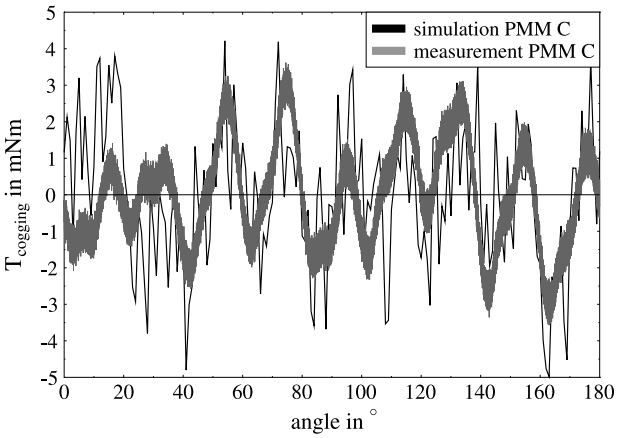

Figure 16: Comparison of measured and simulated results in the time domain.
Bild 16: Vergleich der gemessenen und simulierten Ergebnisse im Zeitbereich.

is larger in the simulation (see next section). Using the positions closer to the stator, an even higher discrepancy would be obtained. The positions closer to the rotor magnets (smaller values for r in Fig. 14) show clearly the influence of the irregular air-gap width due to the shape of the permanent magnets (see also Fig. 11), and are thus discarded as well. As a result, it can be stated, that a position in the centre of the air-gap should be chosen to evaluate Maxwell's stress tensor. Furthermore, more refined techniques for precise torque estimation could be used in the future [14].

The simulation time step is directly linked to the rotational angle of the rotor. By transforming the cogging torque depending on the angle the cogging-torque is analysed in space domain. Figure 15 shows the resulting spectrum. As can be observed, the spectrum includes a larger number of higher harmonics than the measured spectrum. This can be due to a number of reasons, discussed in the following section.

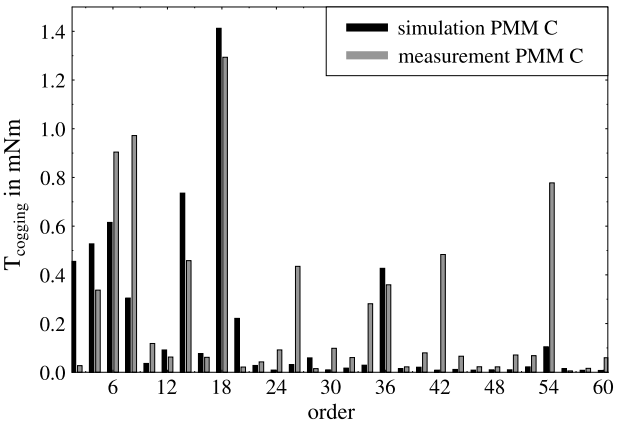

Figure 17: Comparison of the spectra of measured and simulated cogging torque.
Bild 17: Vergleich der Spektren des Rastmoments für Messung und Simulation.

5 Discussion

The comparison of the measured and simulated results is depicted in Fig. 16 for the time domain and Fig. 17 for the spectrum (limited to orders up to $O = 40$). A reasonably good agreement can be noted. Though, the simulation results are likely to have some room for improvement, especially in the mapping of the higher frequent components. The presence of these higher frequency components can be due to numerical instabilities. Nevertheless, the absence of these components in the measured values can also be due to mechanical damping in the measurement setup. The 18^{th} and 36^{th} order are in very good agreement in the simulation and in the measurement. These are also the orders with the maximum value expected by the theory, as explained in the previous section.

6 Conclusion

A setup for an accurate cogging-torque behaviour assessment by means of measurements and simulation has been presented. The measured results, in the time and frequency domain, have been compared to simulated results. A good agreement is achieved. The measurement procedure has proven to be an easy and not too expensive, yet accurate way of measuring cogging torques. The simulation results are expected to reach an even higher accuracy in the near future by improving the torque calculation further and modelling of more relevant machine details. The applied method allows for an improved design process of PMMs analyzing the cogging torque very easily and accurately.

References

[1] Breton, C.; Bartolome, J.; Benito, J. A.; Tassinario, G. ; Flotats, I.; Lu, C. W.; Chalmers, B. J.: Influence of machine symmetry on reduction of cogging torque in permanent-magnet brushless motors. In *IEEE Trans. on Magn*. 36(5), 2000, S. 3819–3823.

[2] Hwang, S.-M.; Eom, J.-B.; Jung, Y.-H.; Lee, D.-W.; Kang, B.-S.: Various design techniques to reduce cogging torque by controlling energy variation in permanent magnet motors. In *IEEE Trans. on Magn*. 37(4), 2001, S. 2806–2809.

[3] Koh, C. S.: Magnetic pole shape optimization of permanent magnet motor for cogging torque reduction. In *IEEE Trans. on Magn*. 33(5), 1997, S. 1822–1827.

[4] Jang, G. H.; Yoon, J. W.; Park, N. Y.; Jang, S. M.: Torque and unbalanced magnetic force in rotational asymmetric brushless DC motors. In *IEEE Trans. on Magn*. 32(5), 1996, S. 5157–5159.

[5] Zienkiewicz, O. C.; Taylor, R. L.: *The finite element method*. McGraw-Hill Book Company, London, 1989.

[6] Kost, A.: *Numerische Methoden in der Berechnung elektromagnetischer Felder*. Springer-Verlag, Berlin, Heidelberg, New York, Barcelona, Budapest, Hong Kong, London, Mailand, Paris, Santa Clara, Singapore, Tokyo, 2000.

[7] van Riesen, D.; Monzel, C.; Kaehler, C.; Schlensok, C.; Henneberger, G.: iMOOSE – an open-source environment for finite-element calculations. In *IEEE Trans. on Magn*. 40(2), 2004, S. 1390–1393.

[8] Aghili, F.; Buehler, M.; Hollerbach, J. M.: Experimental Characterization and Quadratic Programming-Based Control of Brushless-Motors. In *IEEE Trans. on Cont. Syst. Techn*. 11(1), 2003, S. 139–146.

[9] Kikuchi, T.; Kenjo, T.: In-Depth Learning of Cogging/Detenting Torque Through Experiments and Simulations. In *IEEE Trans. on Edu*. 41(4), 1998, S. 352.

[10] Caricchi, F.; Capponi, F. G.; Crescimbini, F.; Solero, L.: Experimental Study on Reducing Cogging Torque and No-Load Power Loss in Axial-Flux Permanent-Magnet Machines with Slotted Winding. In *IEEE, Trans. on Ind. Appl*. 40(4), 2004, S. 1066–1075.

[11] dSPACE: *Solutions for Control* www.dspace.com, 2006.

[12] ANSYS Inc.: www.ansys.com, 2006.

[13] Mizia, J.; Adamiak, K.; et al: Finite Element Force Calculations: Comparison of Methods for Electric Machines. In *IEEE Trans. on Magn*. 24(1), 1988, S. 447–449.

[14] Henrotte, F.; Deliège, G.; Hameyer, K.: The eggshell approach for the computation of electromagnetic forces in 2D and 3D. In *Compel* 23(4), 2004, S. 996–1005.


1


2


3


4


5

1 Dr.-Ing. Christoph Schlensok worked as a research associate from 2001 to 2006 at the Institute of Electrical Machines at RWTH Aachen University. His major fields of activity were the simulation and measurement of electric machinery. Since 2007 he is with Bosch Rexroth AG in Lohr am Main (Germany). He is responsible for the design, calculation, and simulation of induction and synchronous machines as well as torque and linear motors.

Adresse: Bosch Rexroth AG,
Bgm.-Dr.-Nebel-Str. 2, 97816 Lohr am Main,
E-Mail: Christoph.Schlensok@boschrexroth.de

2 Dr.-Ing. Dirk van Riesen is chief engineer of the Institute of Electrical Machines at RWTH Aachen University. He is with the IEM since 1998. Next to administration his major fields of activity are next to simulation and measurement of electric machinery the development of finite-element software.
Adresse: Institut für elektrische Maschinen, RWTH Aachen, Schinkelstr. 4, 52056 Aachen, E-Mail: Dirk.vanRiesen@iem.rwth-aachen.de

3 Dipl.-Ing. Benedikt Schmülling is research associate at the Institute of Electrical Machines at RWTH Aachen University since 2005. His major fields of interest are the design and measurement of electric machinery.
Adresse: Institut für elektrische Maschinen, RWTH Aachen, Schinkelstr. 4, 52056 Aachen, E-Mail: Benedikt.Schmuelling@iem.rwth-aachen.de

4 Dipl.-Ing. Marc Christian Schöning is with the Institute of Electrical Machines at RWTH Aachen University since 2004, working as a research associate. His major fields of activity are the design and simulation of electric machinery. Next to this he is developing software tools for both, the design and simulation of electric machinery.
Adresse: Institut für elektrische Maschinen, RWTH Aachen, Schinkelstr. 4, 52056 Aachen, E-Mail: Marc.Schoening@iem.rwth-aachen.de

5 Univ.-Prof. Dr.-Ing. habil. Dr. h. c. Kay Hameyer is director of the Institute of Electrical Machines at RWTH Aachen University since 2004.
Adresse: Institut für elektrische Maschinen, RWTH Aachen, Schinkelstr. 4, 52056 Aachen, E-Mail: Kay.Hameyer@iem.rwth-aachen.de